CORA Cork Open Research Archive
Cartlann Taighde Oscailte Chorcaí

| | |
|---|---|
| Title | Nanoporous domains in n-InP anodized in KOH |
| Authors | Lynch, Robert P.;O'Dwyer, Colm;Sutton, David;Newcomb, Simon B.;Buckley, D. Noel |
| Publication date | 2007-05-01 |
| Original Citation | Lynch, R. P., O'Dwyer, C., Sutton, D., Newcomb, S. B. and Buckley, D. N. (2007) 'Nanoporous Domains in n-InP Anodized in KOH', ECS Transactions, 6(2), pp. 355-366. doi: 10.1149/1.2731203 |
| Type of publication | Article (peer-reviewed) |
| Link to publisher's version | http://ecst.ecsdl.org/content/6/2/355.abstract - 10.1149/1.2731203 |
| Rights | © 2007 ECS - The Electrochemical Society |
| Download date | 2026-11-08 09:18:34 |
| Item downloaded from | https://hdl.handle.net/10468/6305 |



UCC
University College Cork, Ireland
Coláiste na hOllscoile Corcaigh

# Nanoporous Domains in n-InP Anodized in KOH

R. Lynch,[a] C. O'Dwyer,[b] D. Sutton,[c] S. B. Newcomb[d] and D. N. Buckley[a]

[a] *Department of Physics, and Materials and Surface Science Institute, University of Limerick, Ireland*
[b] *Tyndall National Institute, University College Cork, Ireland*
[c] *Department of Applied Science, Limerick Institute of Technology, Ireland*
[d] *Glebe Scientific Ltd., Glebe Laboratories, Newport, Co. Tipperary, Ireland*

A model of porous structure growth in semiconductors based on propagation of pores along the <111>A directions has been developed. The model predicts that pores originating at a surface pit lead to porous domains with a truncated tetrahedral shape. SEM and TEM were used to examine cross-sections of n-InP electrodes in the early stages of anodization in aqueous KOH and showed that pores propagate along the <111>A directions. Domain outlines observed in both TEM and SEM images are in excellent agreement with the model. The model is further supported by plan-view TEM and surface SEM images. Quantitative measurements of aspect ratios of the observed domains are in excellent agreement with the predicted values.

## Introduction

The formation of pores and porous structures in semiconductors during anodic etching has been extensively studied in a variety of electrolytes.[1-6] Significant progress has been made in understanding basic mechanisms for the formation of porous silicon and several models have been proposed to account for the variety of pore types.[7-8] Most of the work on porous III-V semiconductors has involved acidic electrolytes.[10-12] Orientation of pores along preferred crystallographic directions has been reported under some conditions.[1-17] Porous domains, i.e. laterally confined regions where pores show evident features of organization around a central structure, have been observed in some instances during the early stages of porous layer growth. In GaP,[18-20] semicircular domain cross-sections were observed suggesting isotropic pore growth, while in GaAs[21] the domains were reported to be square in plan view suggesting directionally preferential pore growth.

We recently reported[22-24] the development of nanoporosity in highly doped ($>10^{18}$ $cm^{-3}$) n-InP anodized in 2-10 mol $dm^{-3}$ KOH. We obtained transmission electron microscopy (TEM) and atomic force microscopy (AFM) evidence that the nanoporous region is formed by penetration of surface pits into the semiconductor at particular points and pore propagation originating at these points. TEM cross-sections of electrodes at the early stages of anodization show individual nanoporous domains separated from the surface by a dense, ~40-nm-thick InP layer. We concluded that each domain develops as a result of directionally preferential pore propagation from an individual surface pit that forms a channel through this near-surface layer.

This paper presents results of an investigation of the early stages of pore growth and the resulting domain shape. A model based on pore growth along the <111>A directions

is used to explain the observed structures and domain shapes, and the predictions of the model are compared quantitatively with the experimental observations.

## Experimental

The working electrode and electrochemical cell have been previously described.[23] Briefly, the working electrode consisted of polished (100)-oriented sulfur-doped n-type indium phosphide (n-InP) grown by the liquid-encapsulated Czochralski (LEC) method and supplied by Sumitomo Electric. As-received polished wafers had an essentially featureless surface when viewed at a magnification of 1000X under an optical microscope with Nomarski interference contrast (i.e. a typical surface finish for substrates for epitaxial growth). The nominal density of surface defects of the LEC wafers, as characterized by the etch-pit density (EPD), was in the $10^3$ $cm^{-2}$ range or lower. Wafers were cleaved into coupons (typically ~5 mm square) along the natural {110} cleavage planes and an ohmic contact was made by alloying indium to the back of the coupons. The back and the cleaved edges were electrically isolated from the electrolyte by means of a suitable varnish. The electrode area was typically 0.2 $cm^2$. The carrier concentration was $\sim 3.4 \times 10^{18}$ $cm^{-3}$. The electrolyte was 5 mol $dm^{-3}$ KOH and a conventional three-electrode cell configuration was used employing a platinum counter electrode and saturated calomel electrode (SCE) to which all potentials are referenced. All electrochemical experiments were carried out at room temperature and in the absence of light.

A CH Instruments Model 650A Electrochemical Workstation interfaced to a Personal Computer (PC) was employed for cell parameter control and for data acquisition. All linear potential sweep (LPS) experiments were carried out at a scan rate of 2.5 mV $s^{-1}$. TEM samples were prepared as previously described[25] using a FEI 200 FIB workstation and examined using a JEOL 2000 TEM operating at 200 kV. Cleaved {011} cross-sections were examined using a Hitachi S-4800 field emission scanning electron microscope operating at 5 kV unless otherwise stated. Crystallographic directions were determined by reference to the primary ($0\overline{1}1$) and secondary ($0\bar{1}1$) flats of the supplied wafers (identified using a standard wet chemical[26] etch to reveal the <111>A faces).

## Porous Structure Model

In III-V semiconductors the {111}B planes (e.g. the phosphorous planes in InP) are commonly found to be fast-etching both in electrochemical pore formation[16,17] and in wet etching of trenches.[26] This means that the direction of etching (i.e. the direction in which an etch-front moves or a pore propagates) is the <111>A direction. Gatos and Levine[27,28] have proposed model for the {111} surfaces of III-V semiconductors with a zinc-blende structure. According to this model the etch rates of these surfaces are dependent on the relative reactivity of the terminating atoms where the {111}A plane is terminated by weakly reacting Group III (metallic) atoms and the {111}B is terminated by strongly reacting Group V (non-metallic) atoms. Subsequent work by Holt[29] into the behavior of these surfaces in InSb supports this model, showing a strong reactivity for the Sb and a weaker reactivity for the In. Substantial research into the behavior of GaAs[30-32] and InP[33,34] in a range of etchants, such as Piranha ($H_2SO_4$-$H_2O_2$-$H_2O$ mixtures) and bromine-methanol, has identified the {111}A planes as the slow etch planes that are revealed during chemical etching. Similar results for photoelectrochemical etching[35,36] and thermal

decomposition[37] of InP have shown the {111}A planes to be revealed due to the preferential removal of phosphorus.

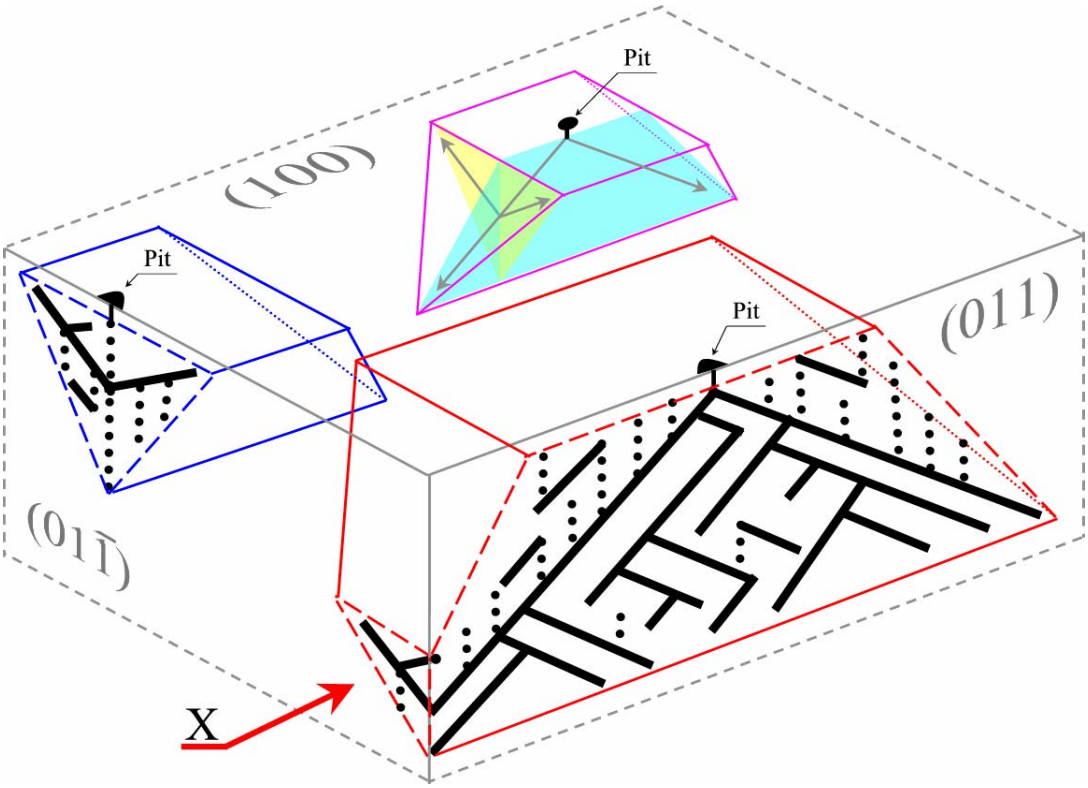



Figure 1: Isometric drawing of porous domains predicted for pore growth along the <111>A directions. The trapezium-shaped and triangular cross-sections in the (011) and (01$\bar{1}$) cleavage planes, respectively, are shown. Where the (01$\bar{1}$) cleavage plane intersects a domain near one of its vertices, the resulting small triangular cross-section (X) appears at a distance from the surface: an example is seen at X in Fig. 3.

We showed in an earlier paper[24] that porous domains form in the early stages of anodization of InP in KOH and that each domain originates from a pit in the surface. We now consider preferential growth along the <111>A directions of pores originating at a surface pit and show how we can deduce the shape of the resulting porous domains. In order to do this, it is useful to first consider the hypothetical case of pores originating at a point in the interior of a crystal and advancing only along the <111>A directions. If branching of pores does not occur and if pores grow at a instantaneously homogenous rate for all pores, after a time, t, pores will have grown an equal distance, $l = \int_0^t v\,dt$, along each of the four <111>A directions. These primary pores will form the vertices of a tetrahedron and if branching is allowed to occur along the <111>A directions this tetrahedron will fill completely with pores up to its surfaces. Of course the domain originates not from a point in the bulk of the semiconductor but from a point near the surface of the electrode, and therefore only one half of the tetrahedron can exist. As shown in Fig. 1 the truncated tetrahedral shape, produced by the proposed model, has trapezium-, triangle- and square-shaped cross-sections in (011), (01$\bar{1}$) and (100) planes, respectively, where the (100) cross-section is of the domain base.

## Results and Discussion

### Cross-sectional Microscopy

To develop a three-dimensional understanding of the growth of these porous-structures, images were taken of three orthogonal views: the (100) surface plane, the (011) cleavage plane (parallel to primary flat) and the (01$\bar{1}$) cleavage plane (parallel to secondary flat). Fig. 2 shows an SEM (011) cross-section from an InP electrode in the early stages of anodization. A trapezium-shaped nanoporous domain (indicated by the broken line) is observed. The domain is separated from the surface by a near-surface layer of dense InP (at A). The similarity to the trapezium-shaped domain cross-section in the (011) plane in Fig. 1 is clearly evident. Primary pores extend downwards along the <111>A direction from a point near the surface to the bottom corners of the trapezium (see the pore marked 'B' on the left and a similar pore symmetrically on the right) Other pores branch downwards along the <111>A directions from the primary pores and fill the region between the primary pores. In contrast, the region between the primary pores and the near-surface layer has much fewer in-plane pores and is occupied mainly by holes. These holes can be seen in the (011) cross-section of the schematic in Fig. 1 and are the cross-sections of <111>A pores growing within orthogonal (01$\bar{1}$) planes.

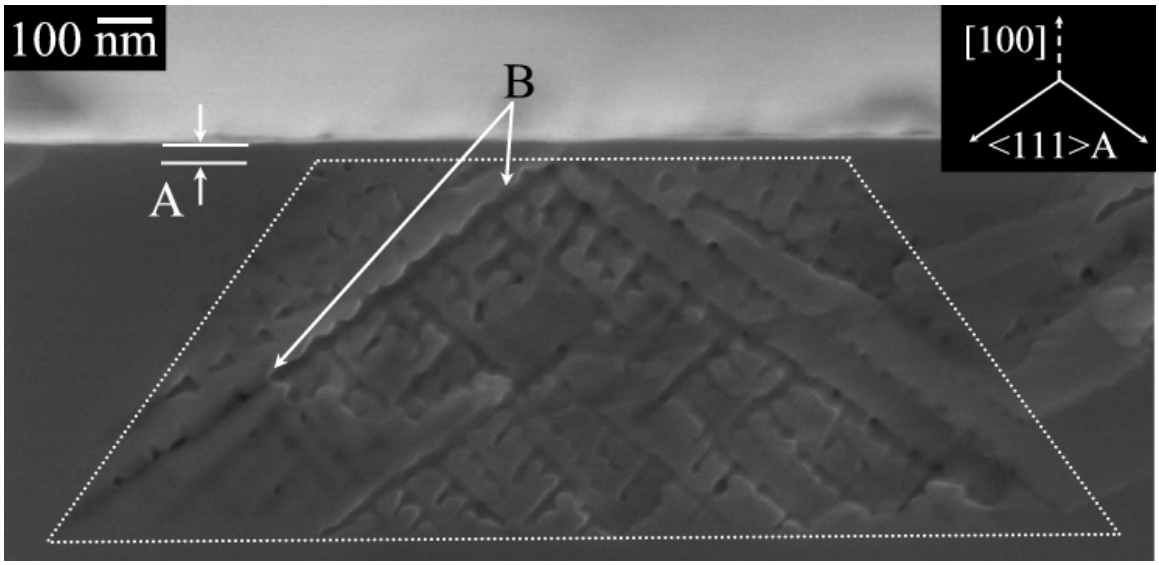



Figure 2: Cross-sectional SEM image of InP cleaved along the (011) plane following an LPS from 0 to 0.44 V (SCE) at 2.5 mV $s^{-1}$ in 5 mol $dm^{-3}$ KOH. Pore growth along the <111>A directions and trapezium-shaped domain are visible.

Fig. 3 shows an SEM image of the (01$\bar{1}$) plane of an InP electrode in the early stages of anodization. A triangular domain cross-section can be seen in the image corresponding to the (01$\bar{1}$) cross-section shown in Fig. 1. Vertical arrays of holes can be seen corresponding to the cross-sections in this plane of the <111>A pores growing down from the surface in (011) planes as observed in Fig. 2. As can be seen in the schematic in Fig. 1, the <111>A directions in this plane, the (01$\bar{1}$) plane, are upwards towards the surface (making an angle of 35.26° with it). Pores along these directions seen in Fig. 3, are similar in orientation to those represented schematically in the (01$\bar{1}$) cross-section in Fig. 1. Thus we can see from Figs. 2 and 3 that pores grow downwards from the surface

along the <111>A directions in the (011) plane and upwards along the <111>A directions in the (01$\bar{1}$) plane giving patterns in the SEM cross-sections very closely resembling those represented schematically in the corresponding cross-sections in Fig. 1.

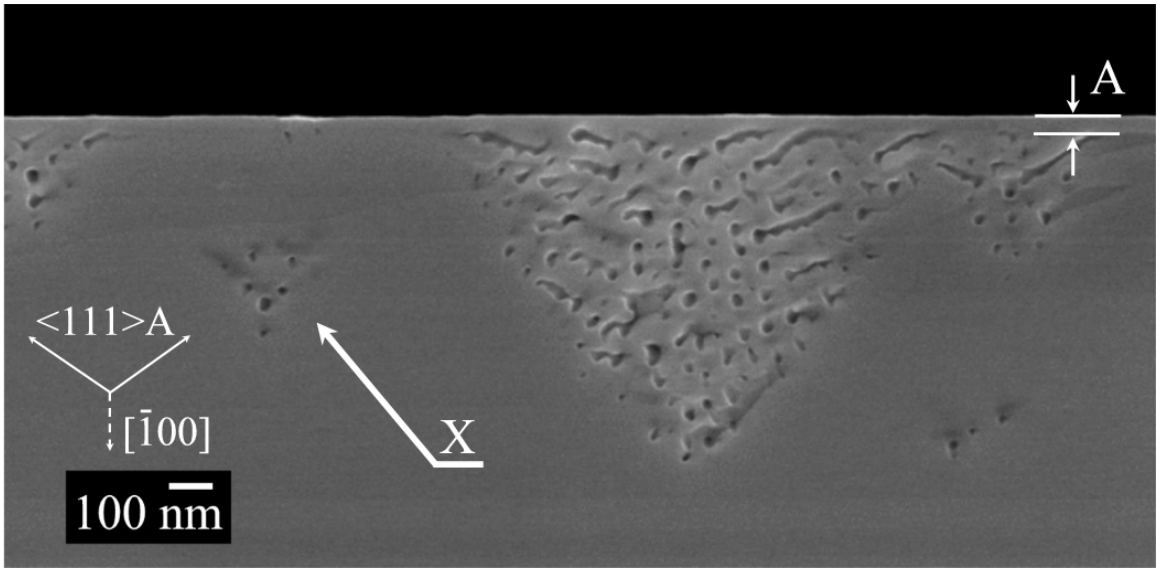



Figure 3: Cross-sectional SEM image of InP cleaved along the (01$\bar{1}$) plane (orthogonal to Fig. 2) following an LPS from 0 to 0.44 V (SCE) at 2.5 mV $s^{-1}$ in 5 mol $dm^{-3}$ KOH. Pore growth along the <111>A directions and a triangular domain are clearly visible. A smaller domain cross-section at a distance from the surface is also visible (at X).

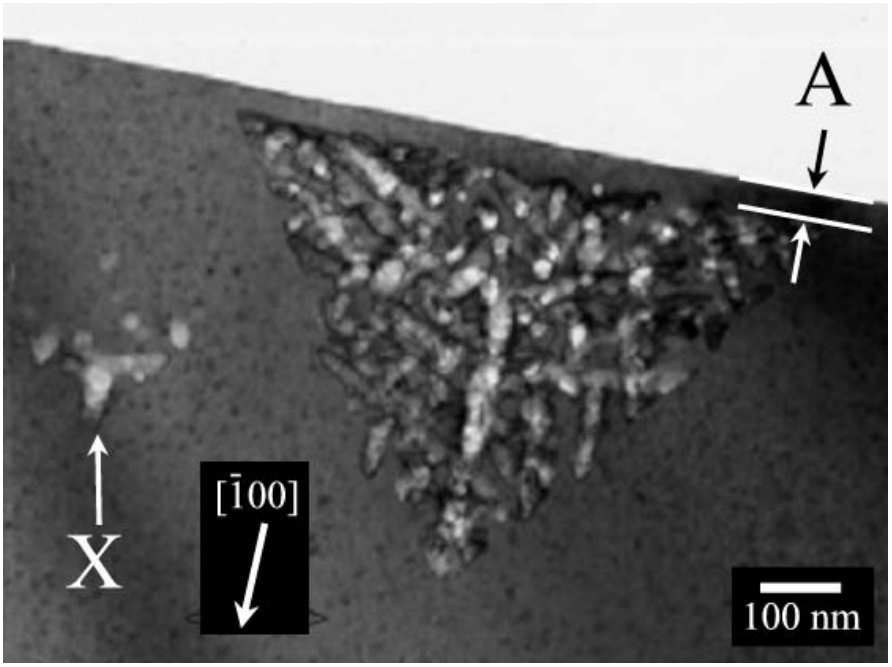



Figure 4: Cross-sectional TEM image of InP after an LPS from 0.0 to 0.44 V (SCE) in 5 mol $dm^{-3}$ KOH at 2.5 mV $s^{-1}$ (Same conditions as Fig. 3). The TEM slice is ~100 nm thick; the [$\bar{1}$00] direction is shown by an arrow.

Fig. 4 shows a TEM cross-section of an electrode similar to that in Fig. 3. Again, it can be seen that the porous domain has a triangular outline and the dense near-surface layer is more clearly defined (at A). However, the interior of the image has a different appearance to that of the corresponding SEM image in Fig. 3. This difference is due to a TEM image being a two-dimensional representation of a three-dimensional slice of material. It follows that overlapping pores appear as if they are intersecting and pores that are growing through the volume appear as if they are growing within the plane of the image. This projection of images from the third dimension (depth of the slice) effectively prevents direct observation of the actual pore direction. Therefore, in Fig. 4 the prominent feature the [$\bar{1}$00] central axis of the domain and parallel [$\bar{1}$00] features, which are at intervals of ~40 nm, correspond to planes of pores growing in the orthogonal (011) planes and to the vertical arrays of holes in Fig. 3.

In both the SEM (Fig. 3) and TEM (Fig. 4) images of the (01$\bar{1}$) cross-section, a small triangular feature (marked X in each case) at a considerable distance from the surface is clearly observed. It is clear that this is a cross-section of a domain that intersects the (01$\bar{1}$) cleavage plane close to one of its corners as shown at X in Fig. 1. This provides further confirmation that the nanoporous domains have a truncated-tetrahedron shape.

**Plan-view Microscopy**

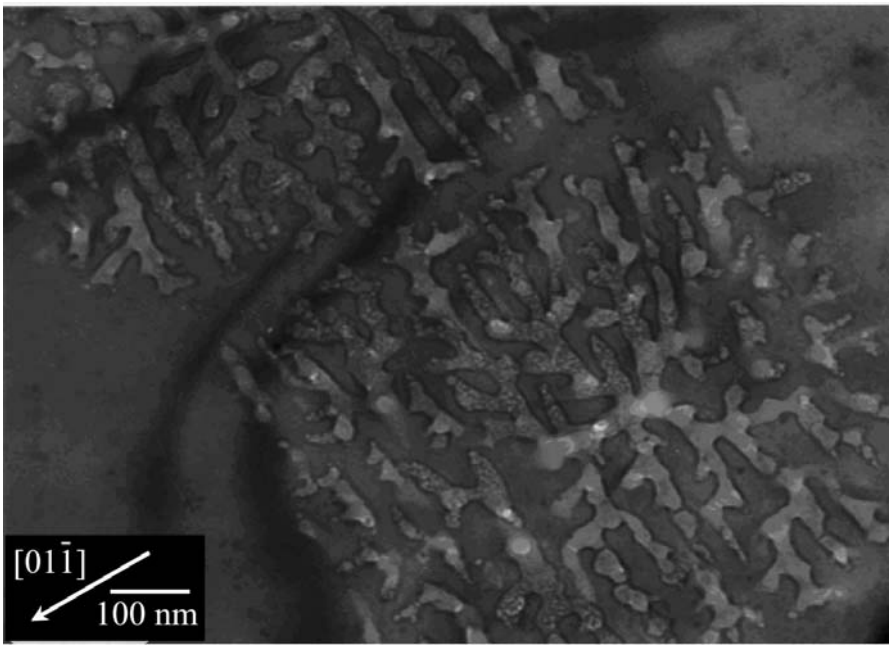



Figure 5: Plan-view TEM image of a ~100-nm-thick section taken from the surface of the same InP electrode as in Fig. 4. The plane of the micrograph is (100).

Fig. 5 shows a plan-view TEM image of a 100-nm-thick slice along the (100) plane taken from the surface of an electrode. A nanoporous region with a square outline is clearly visible. This is consistent with the shape of the domain in Fig. 1 which shows a square base parallel to the surface of the electrode and immediately below the near-surface layer. The porosity within the square-shaped outline of the domain base appears as a mesh of approximately orthogonal structures. These are approximately parallel to the sides of the square and correspond to the <011> directions. Thus, the mesh represents the

projection on the (100) plane of pores along the <111>A directions, again consistent with Fig. 1.

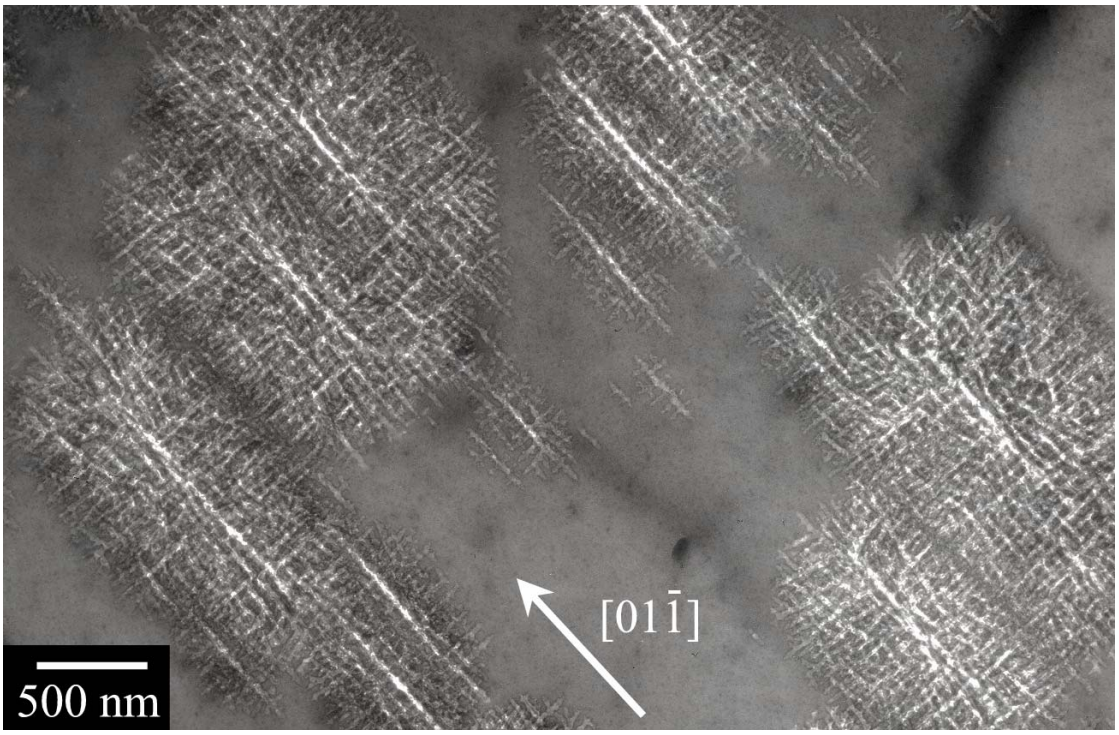


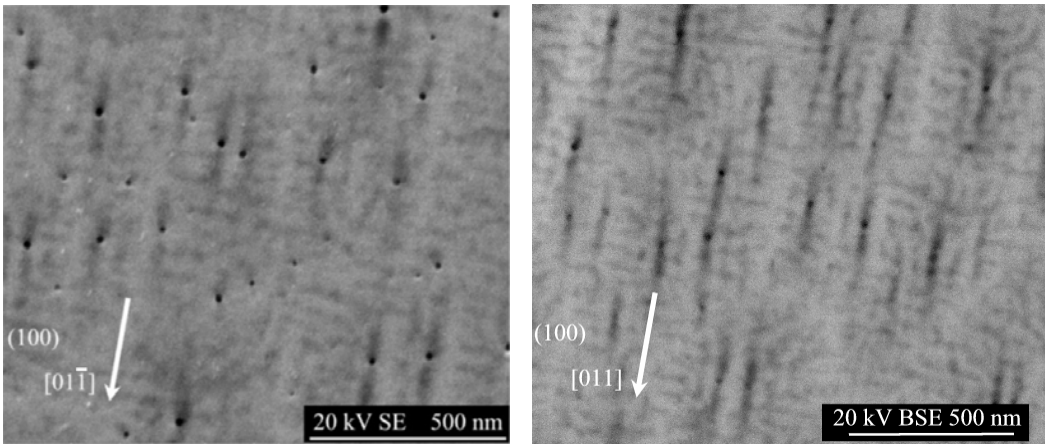

Figure 6: Plan-view TEM image of a ~400-nm-thick section taken from the surface of the same InP electrode as in Fig. 3. The plane of the micrograph is (100).

Due to the thinness of the slice in Fig. 5, only the near-surface part (i.e. the square base) of the porous structure could be observed. When a thicker slice is examined it is possible to view the overall outline of domains in plan-view and not just the base of the domain. Fig. 6 shows such an image where some of the domains are small enough to be completely within the thickness of the TEM slice. (The section thickness is ~400 nm which is thicker than some, but not all, of the domains at this stage of etching.) In this image it can be seen that the domains are terminated at points in the long direction and by flat edges in the short direction, similar to the outline of a ship's deck and corresponding to the overall domain shape of a truncated tetrahedron (see Fig. 1). Again, the pores within the domains are aligned in a mesh along the <011> axes corresponding to planes of pores growing along the <111>A directions.

Fig. 7a is a SEM secondary-electron image of the surface of an electrode that has been anodically etched. The electron energy is sufficiently high (20 keV) to allow both the surface and near sub-surface features of the electrode to be examined. As previously observed by AFM[24] the etching has caused small pits to appear in the surface. As observed in Fig. 7a, these pits are approximately circular with a typical diameter of 20 nm.

Fig. 7b is a SEM backscattered-electron image of the same electrode. The image highlights sub-surface structures similar to the structures that are visible in Fig. 7a as pronounced dark primary stripes pointing from the surface-pits along the [01$\bar{1}$] and [0$\bar{1}$1]

crystallographic directions, and less pronounced secondary stripes extending orthogonally away from the primary stripes. This mesh of orthogonal stripes along the <011> axes of the image corresponds to the <011> structures seen in TEM plan views (Fig. 5). They are the projections in the (100) plane of pores along the <111>A direction.




(a) (b)

Figure 7: (a) Secondary-electron and (b) backscattered-electron SEM images of (100) InP surface following a LPS from 0.0 to 0.537 V (SCE) in 5 mol $dm^{-3}$ KOH at 2.5 mV $s^{-1}$. Both images were taken at 20 kV allowing surface pits and some sub-surface features to be visible.

**Comparison of Experimental and Theoretical Domain Shapes**

Fig. 8 shows a schematic representation of domain cross-sections predicted (Fig. 1) for the two orthogonal {011} planes that contain the central [100] axis of a domain. Each of the schematics shows the outline of a domain that has grown for a time t from an origin point just beneath the surface.

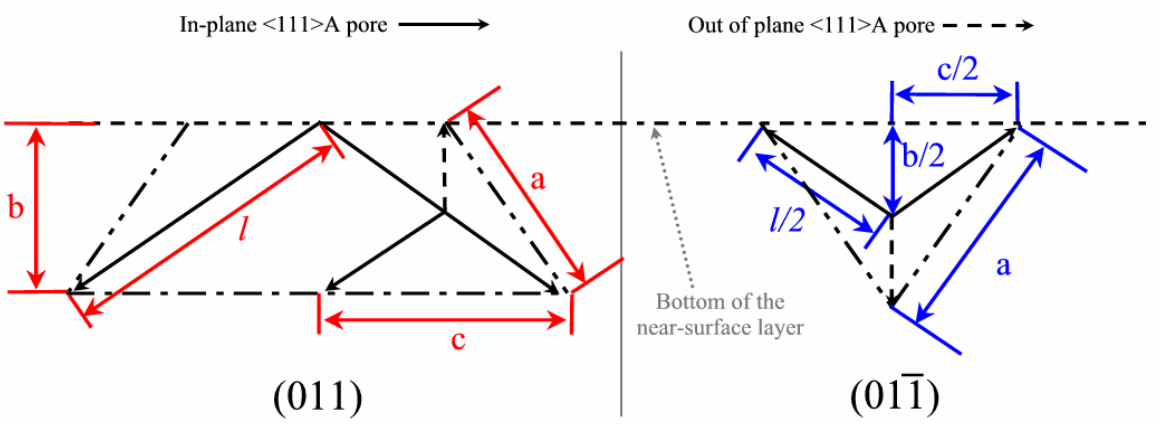



Figure 8: Schematic representation of {011} cross-sections along the central [100] axis through a domain from Fig. 1.

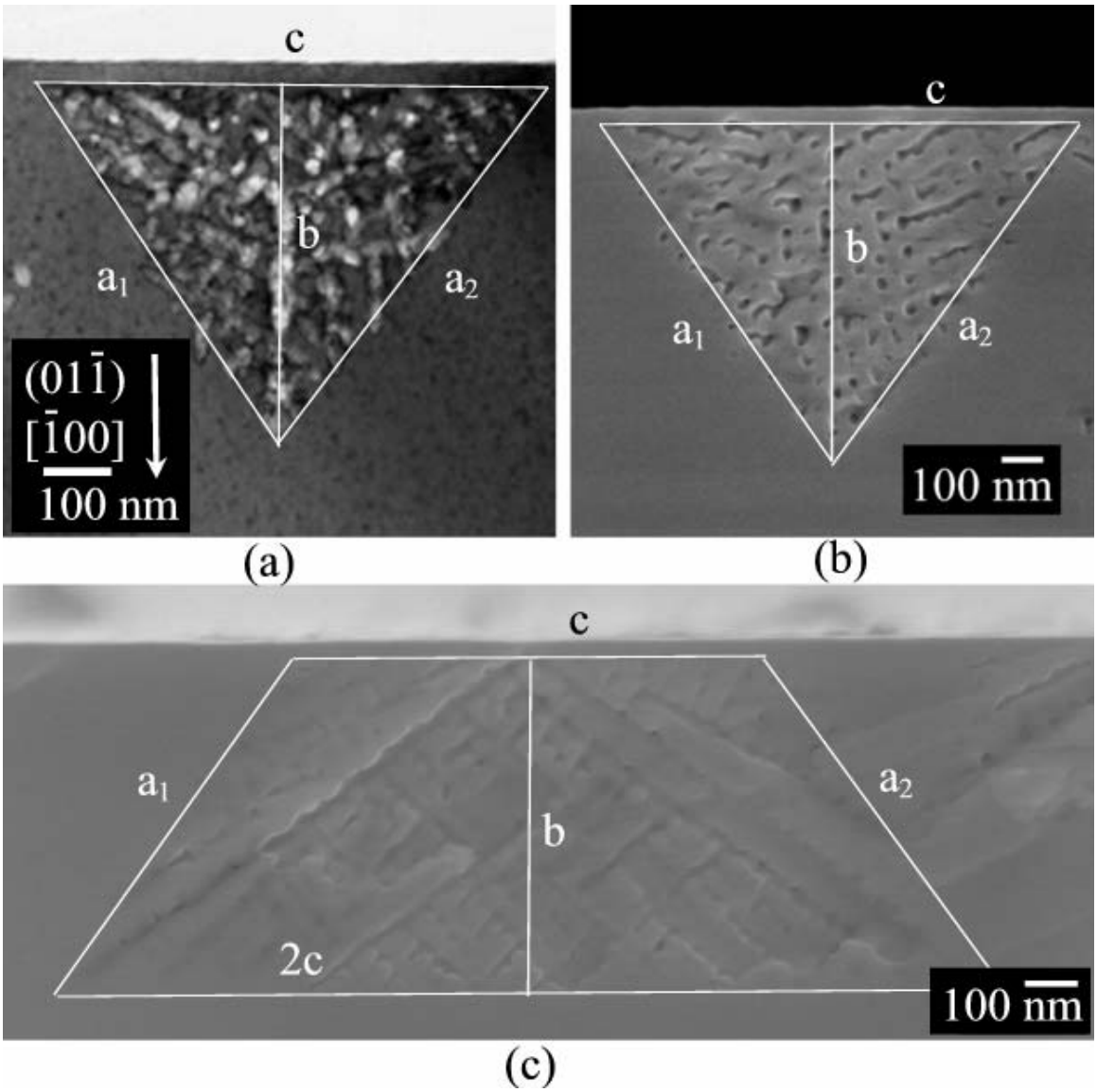



Figure 9: Micrographs showing where the measurements for Table 1 were obtained. (a) TEM image in Fig. 4; (b) SEM image in Fig 3; and (c) SEM image in Fig 2.

After a time t, the main pores in a domain (running from the central point to a vertex) will have grown a length, *l*. Since *l* is along a <111> direction, the domain depth *b* and the width of the domain base *c* (half the length of the long edge of the trapezium) are the components of *l* along the <100> and <011> directions, respectively. Thus, *l* is the diagonal of a cube of side *b* and *c* is the diagonal of the cube face. It follows that

$$b = l\sqrt{1/3}$$

$$c = l\sqrt{2/3} = b\sqrt{\frac{3}{1}}\sqrt{\frac{2}{3}} = b\sqrt{2}$$

and the side *a* of the cross-section is

$$a = \sqrt{b^2 + \left(\frac{c}{2}\right)^2} = \sqrt{b^2 + \frac{b^2}{2}} = b\sqrt{3/2}$$

Thus, the predicted value of the width-to-depth ratio is $\frac{c}{b} = \sqrt{2} = 1.414$. Similarly, the ratio $\frac{a}{c} = \frac{\sqrt{3}}{2} = 0.866$. These ratios are valid for any $(01\bar{1})$ domain cross-section but they are only valid for (011) domain cross-sections that include the central axis of the domain (where a cleave contains the surface pit of the domain).

Measurements taken from TEM and SEM {011} domain cross-sections in this paper are shown in Table 1 (see Fig. 9). The ratios of these values are also shown along with the corresponding theoretical values. It can be seen that there is excellent agreement between the experimental and theoretical values. This supports the hypothesis that the pore growth occurs preferentially along the <111>A crystallographic directions. Thus, there is conclusive evidence that the domain cross-sections shown in the TEM and SEM micrographs in this paper are cross-sections of square-based truncated tetrahedral domains resulting from the propagation of pores from individual pits preferentially along the <111>A directions.

Table 1: Comparison of experimental and theoretical ratios for the dimensions of porous domains. The superscript letters a, b and c, refer to the respective images in Fig. 9.

| | **Measured Value / nm (Triangle) [a]** | **Measured Value / nm (Triangle) [b]** | **Measured Value / nm (Trapezium) [c]** | **Predicted Value** |
|---|---|---|---|---|
| $a_1$ | 794 | 949 | 787 | $l\sqrt{\frac{1}{2}}$ |
| $a_2$ | 805 | 978 | 783 | $l\sqrt{\frac{1}{2}}$ |
| $b$ | 650 | 785 | 643 | $l\sqrt{\frac{1}{3}}$ |
| $c$ | 919 | 1111 | 903 | $l\sqrt{\frac{2}{3}}$ |
| $2c$ | n/a | n/a | 1810 | $l\sqrt{\frac{8}{3}}$ |
| $\frac{c}{b}$ | 1.413 | 1.415 | 1.404 | 1.414 |
| $\frac{2c}{(2\times b)}$ | n/a | n/a | 1.407 | 1.414 |
| $\frac{a1}{\langle c \rangle}$ | 0.863 | 0.854 | 0.870 | 0.866 |
| $\frac{a2}{\langle c \rangle}$ | 0.876 | 0.880 | 0.866 | 0.866 |

## Conclusions

We have developed a model of porous structure growth in semiconductors based on propagation of pores along the <111>A directions. The model predicts that such pores, originating at a surface pit and propagating at an instantaneously homogenous growth rate, lead to porous domains with a truncated tetrahedral shape. The domains have trapezium-, triangle- and square-shaped cross-sections in the (011), (01$\bar{1}$) and (100) planes, respectively. We have used SEM and TEM to examine cross-sections of n-InP electrodes in the early stages of anodization in aqueous KOH. Cross-sectional SEM images show that pores originating from surface pits propagate along the <111>A directions while TEM images show projections of <111>A pores. Domain outlines observed in both TEM and SEM images are in excellent agreement with the model. The model is further supported by plan-view TEM and surface SEM images. Quantitative measurements of aspect ratios of the observed domains are in excellent agreement with the predicted values.

## References


1. R.L. Smith and S.D. Collins, *J. Appl. Phys*., **71**, 8 (1992)
2. H. Föll, J. Carstensen, S. Langa, M. Christophersen and I.M. Tiginyanu, *phys. stat. sol. (a)* **197**, 61 (2003)
3. G. Oskam, A. Natarajan, P.C. Searson and F.M. Ross, *Appl. Surf. Sci*., **119,** 160 (1997)
4. S. Langa, J. Carstensen, I.M. Tiginyanu, M. Christophersen and H. Föll, *Electrochem. Solid-State Lett.* **4,** G50 (2001)
5. S. Langa, J. Carstensen, I.M. Tiginyanu, M. Christophersen and H. Föll, *Electrochem. Solid-State Lett.* **3,** 514 (2000)
6. E. Harvey, C. O'Dwyer, T. Melly, D.N. Buckley, V.J. Cunnane, D. Sutton, S.B. Newcomb and S.N.G. Chu, in *State-of-the-Art Program on Compound Semiconductors XXXV*, P.C. Chang, S.N.G. Chu and D.N. Buckley, Editors, PV **2001-20**, p. 87, The Electrochemical Society, Proceedings Series Pennington, NJ (2001)
7. X.G. Zhang, *J. Electrochem. Soc.* **151**, C69 (2004)
8. J. Carstensen, M. Christopersen and H. Föll, *Mater. Sci. Eng. B* **69-70**, 23 (2000)
9. J. Carstensen, M. Christopersen, G Hasse and H. Föll, *phys. stat. sol. (a)* **182**, 63 (2000)
10. H. Föll, J. Carstensen, S. Langa, M. Christophersen and I.M. Tiginyanu, *Adv. Mater.* **15**, 183 (2003)
11. P. Schmuki, L. Santinacci, T. Djenizian and D.J. Lockwood, *phys. stat. sol. (a)* **182,** 51 (2000)
12. P. Schmuki, L.E. Erickson, D.J. Lockwood, B.F. Mason, J.W. Fraser, G. Champion and H.J. Labbé, *J. Electrochem. Soc.* **146,** 735 (1999)
13. M.M. Faktor, D.G. Fiddyment and M.R. Taylor, *J.Electrochem. Soc.* **122**, 1566 (1975)
14. F.M. Ross, G. Oskam, P.C. Searson, J.M. Macaulay and J.A. Liddle, *Philos. Mag. A* **75**, 2 (1997)
15. C. O'Dwyer, D.N. Buckley, V.J. Cunnane, D. Sutton, M. Serantoni and S.B. Newcomb, in *Proceedings of the State-of-the-Art Program on Compound*

*Semiconductors XXXVII*, PV **2002-14**, p. 259, The Electrochemical Society, Proceedings Series, Pennington, NJ (2002)
16. S. Langa, J. Carstensen, I.M. Tiginyanu, M. Christophersen and H. Föll. *Electrochem. Solid-State Lett.* **5**, C-14 (2002)
17. E. Speicker, M. Rudel, W. Jäger, M. Leisner and H. Föll, *phys. stat. sol. (a)* **202,** 2950 (2005)
18. B.H. Erné, D. Vanmaekelbergh and J.J. Kelly, *J. Electrochem. Soc.* **143**, 305 (1996)
19. B.H. Erné, D. Vanmaekelbergh and J.J. Kelly, *Adv. Mater.* **7**, 739 (1995)
20. R.W. Tjerkstra, J. Gómez Rivas, D. Vanmaekelbergh and J.J. Kelly, *Electrochem. Solid-State Lett.* **5**, G32 (2002)
21. I.M. Tiginyanu, C. Schwab, J.-J. Grob, B. Prevot, H.L. Hartnagel, A. Vogt, G. Irmer and J. Monecke, *Appl. Phys. Lett*. **71**, 3829 (1997)
22. R. Lynch, C. O'Dwyer, D.N. Buckley, D. Sutton and S.B. Newcomb, *ECS Trans* **2**, 131 (2006)
23. C. O'Dwyer, D.N. Buckley, D. Sutton, and S.B. Newcomb, *J. Electrochem. Soc.* **153,** G1039 (2006)
24. C. O'Dwyer, D.N. Buckley, D. Sutton, M. Serantoni, and S.B. Newcomb, *J. Electrochem. Soc.,* **154**, H78 (2007)
25. L. A. Giannuzzi and F. A. Stevie, *Micron.* **30**, 197 (1999)
26. M. Kappelt and D. Bimberg, *J. Electrochem. Soc.* **143**, 3271 (1996)
27. H.C. Gatos and M.J. Lavine, *J. Electrochem. Soc.* **107**, 427 (1960)
28. H.C. Gatos, *J. Appl. Phys* **32** (7), 1232 (1961)
29. D.B. Holt, *J. Appl. Phys* **31**, 2231 (1960)
30. S. Iida and K. Ito, *J. Electrochem. Soc.* **118** (5), 768 (1971)
31. Y. Tarui, Y. Komiya and Y. Harada, *J. Electrochem. Soc.* **118** (1), 118 (1971)
32. S. Adachi and K. Oe, *J. Electrochem. Soc.* **130**, 2427 (1983)
33. P.H.L. Notten, *J. Electrochem. Soc.* **138**, 243 (1991)
34. I.E. Vermeir, W.P. Fomes and P. van Daele, *J. Electrochem. Soc.* **142**, 3226 (1995)
35. D. Soltz and L. Cescato, *J. Electrochem. Soc.* **143**, 2815 (1996)
36. M.M. Carrabba, N.M. Nguyen and R.D. Rauh, *J. Electrochem. Soc.* **134**, 1855 (1987)
37. S.N.G. Chu, C.M. Jodlauk and W.D. Johnston, Jr., *J. Electrochem. Soc.* **130**, 2399 (1983)